Electronic Supplementary Material (ESI) for Physical Chemistry Chemical Physics.

Supplementary Information

Selenylation to charge transfer improvement at the counter electrode (CE)/electrolyte interface for nanocrystalline $Cu_{1.8}S_{1-x}Se_x$ CEs

Z.Z. Liu[a], K.P. Li[a], X.B. Yang[b], Y.Q. Zhang[a], Z.X. Xie[a], Z.Q. Duan[a], B. Zhou[a], Y.M. Hu[a,*]

[a] College of Engineering, Dali University, Dali, 671003, China

[b] Faculty of Materials Science and Engineering, Kunming University of Science and Technology, Kunming, 650093, China

1. Synthesis of nanocrystalline $Cu_{1.8}S$ and $Cu_{1.8}S_{1-x}Se_x$ and fabrication of the CEs

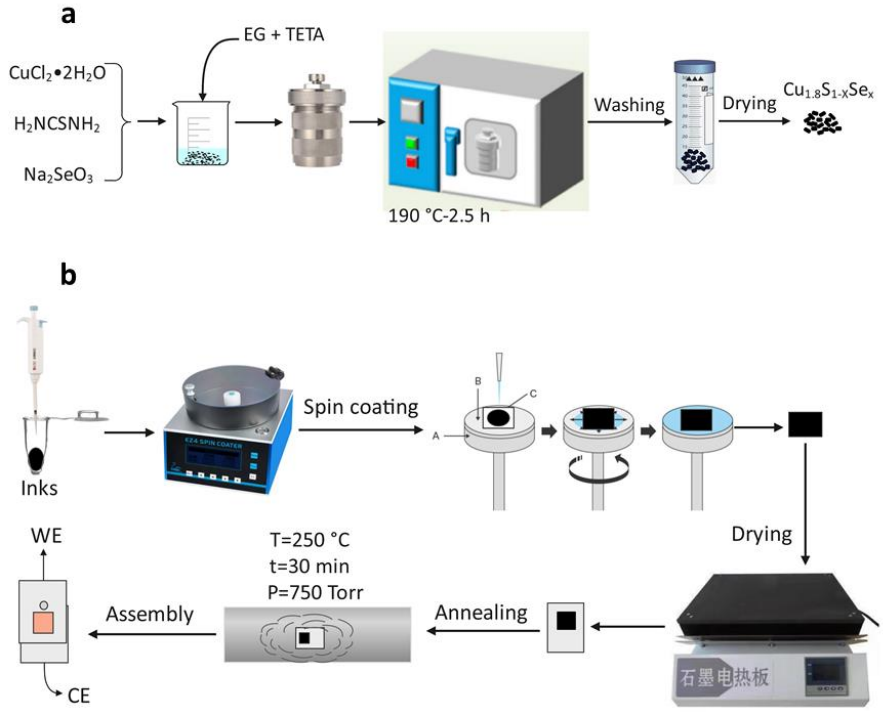

Figure S1. *Schematic diagrams of the synthesis of nanocrystalline $Cu_{1.8}S$ and $Cu_{1.8}S_{1-x}Se_x$ (a), and fabrication of the CEs (b).*

The reaction in the preparation of $Cu_{1.8}S$ can be expressed as follows [1]:

$$2CuCl_2 + CH_4N_2S + H_2O \longrightarrow 2CuCl + S + 2HCl + NH_2CONH_2$$

$$CH_4N_2S + 3H_2O \longrightarrow H_2S + 2NH_4^+ + CO_3^{2-}$$

$$Cu^{2+} + H_2S \longrightarrow CuS + 2H^+$$

$$8CuCl + CuS + 4H_2S \longrightarrow Cu_9S_5 + 8HCl$$

2. XRD patterns of the $Cu_{1.8}S_{1-x}Se_x$ CEs prepared by nanocrystalline $Cu_{1.8}S_{1-x}Se_x$ powder

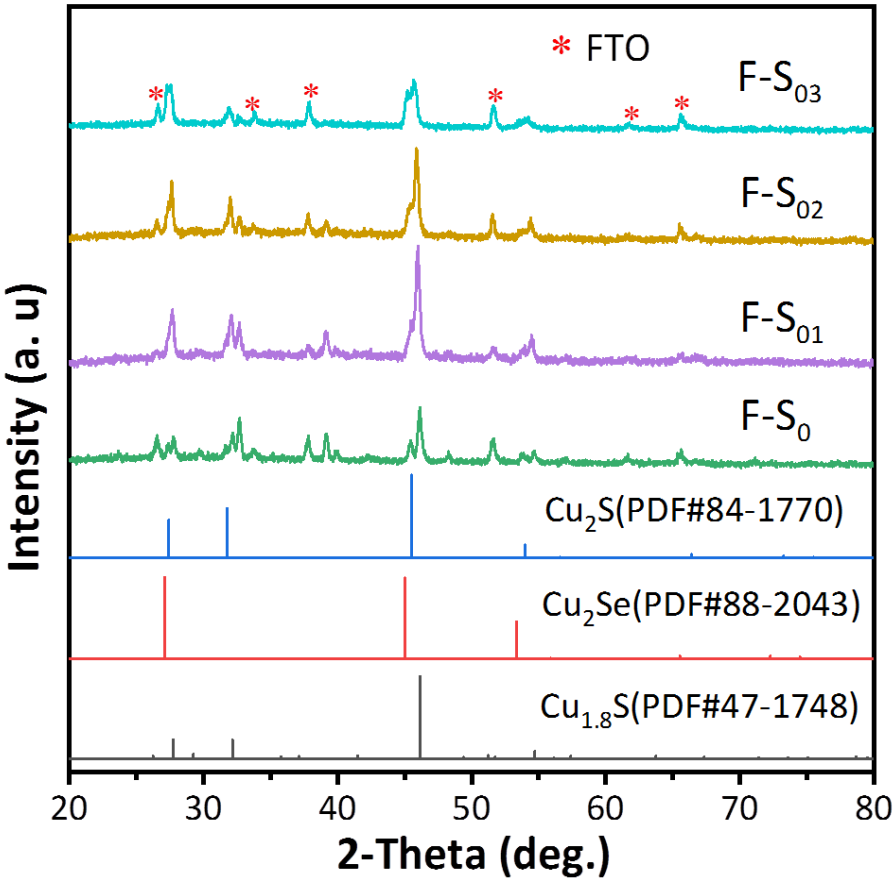

Figure S2. *XRD patterns of the CEs of F-S_0, F-S_{01}, F-S_{02} and F-S_{03}.*

After annealing at 250 °C for 30 min, in addition to the peaks distinct in the precursor powder, Cu_2S arises in F-S_0. During the annealing, partial S was evaporated and the relatively rich Cu in the lattice together with the remaining S formed the Cu_2S.

3. TEM images of the as-prepared powder samples of S_0 and S_{02}

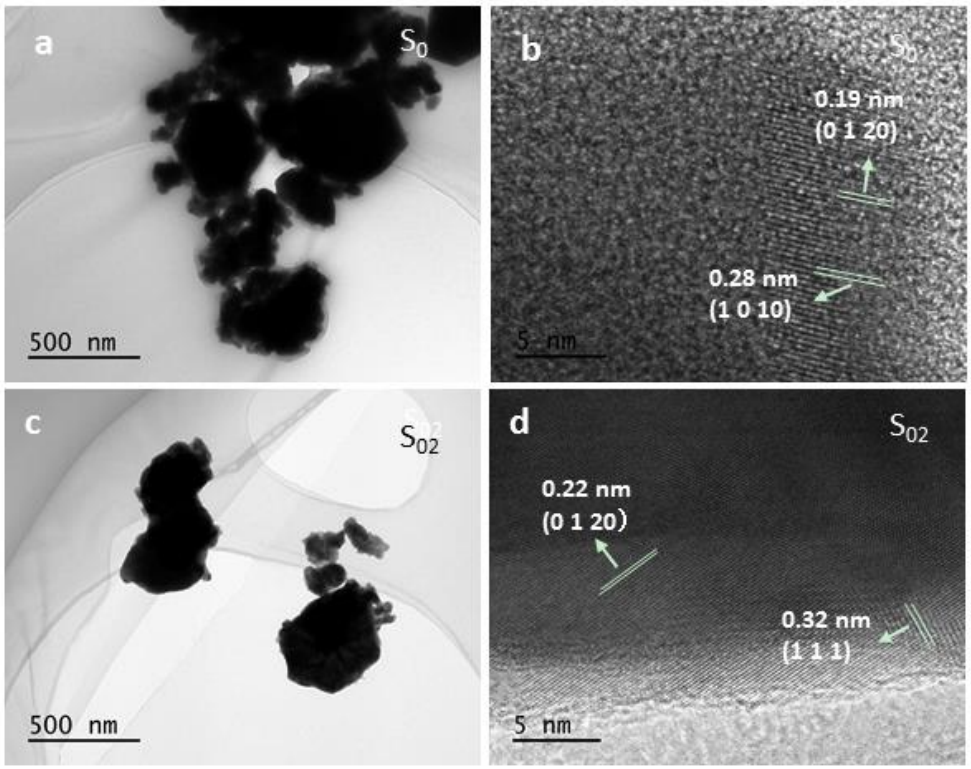

Figure S3. *TEM images of S_0 and S_{02}.*

4. Specific surface areas of the powder samples of S_0 and S_{02}

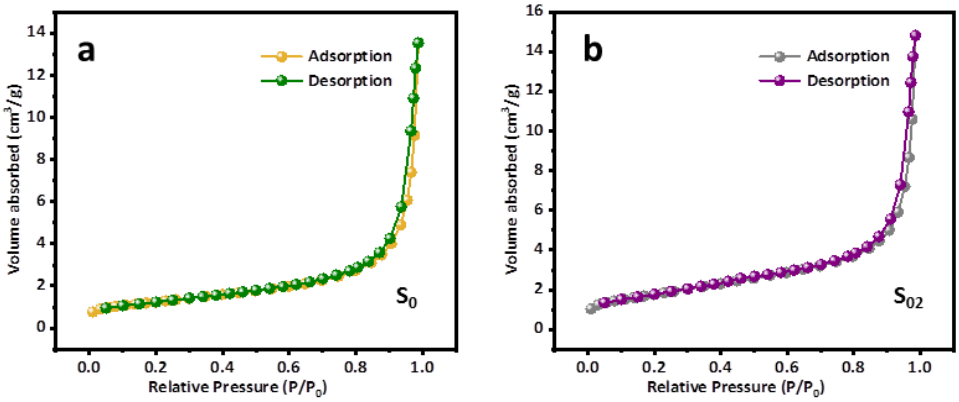

Figure S4. *Adsorption and desorption curves of of S_0 (a) and S_{02} (b).*

5. The Valence band maximum (VBM) of the CEs

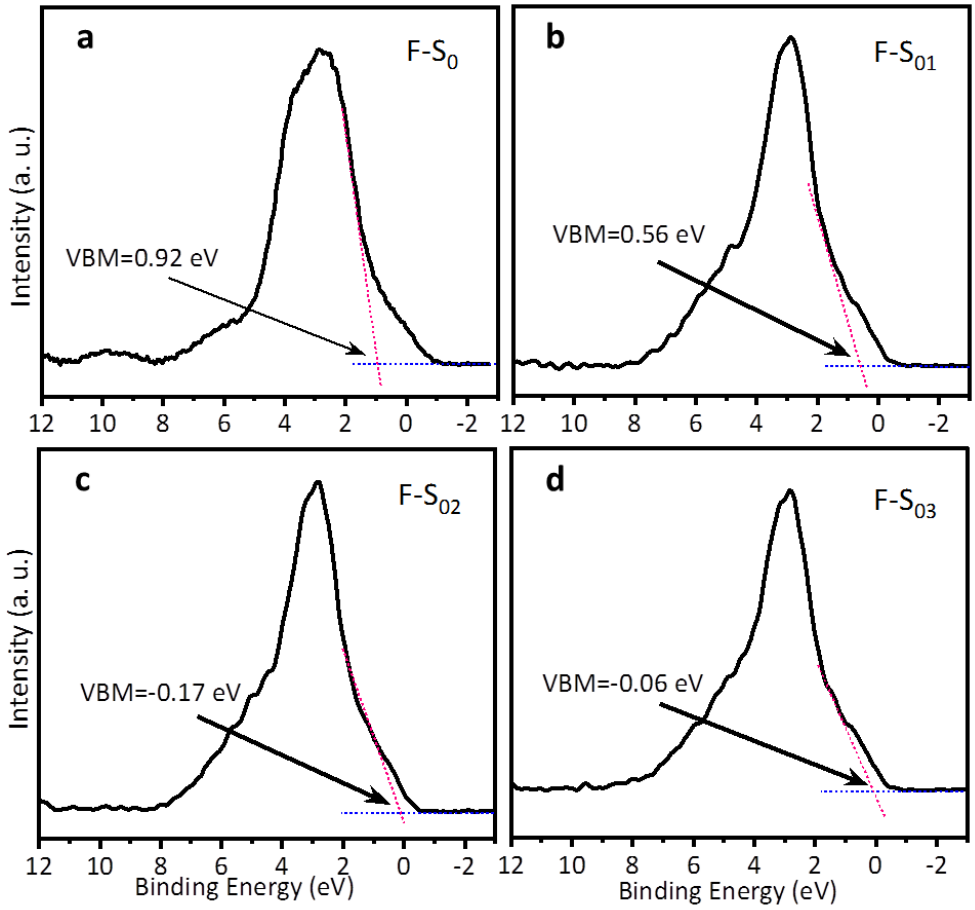

Figure S5. *VB-XPS plots of the CEs F-S_0, F-S_{01}, F-S_{02} and F-S_{03}.*

6. Properties of the $Cu_{1.8}S_{1-x}Se_x$ CEs prepared by selenylation of $Cu_{1.8}S$ films

6.1 Selenylation of $Cu_{1.8}S$ films to $Cu_{1.8}S_{1-x}Se_x$ CEs

In this process, $Cu_{1.8}S_{1-x}Se_x$ CEs were prepared by selenylation of $Cu_{1.8}S$ films fabricated using the same process depicted in the manuscript, that is, $Cu_{1.8}S$ films were first spin-coated onto FTO surfaces. Then, different amounts of selenium powder (0 mg/50 mg/100 mg/150 mg) were added during the film annealing process for selenylation at 550 °C for 15 min under nitrogen atmosphere. The CEs were named as F-CS_0, F-CS_1, F-CS_2, F-CS_3, respectively. Schematic diagram of the fabrication

of the CEs are shown in Fig. S4

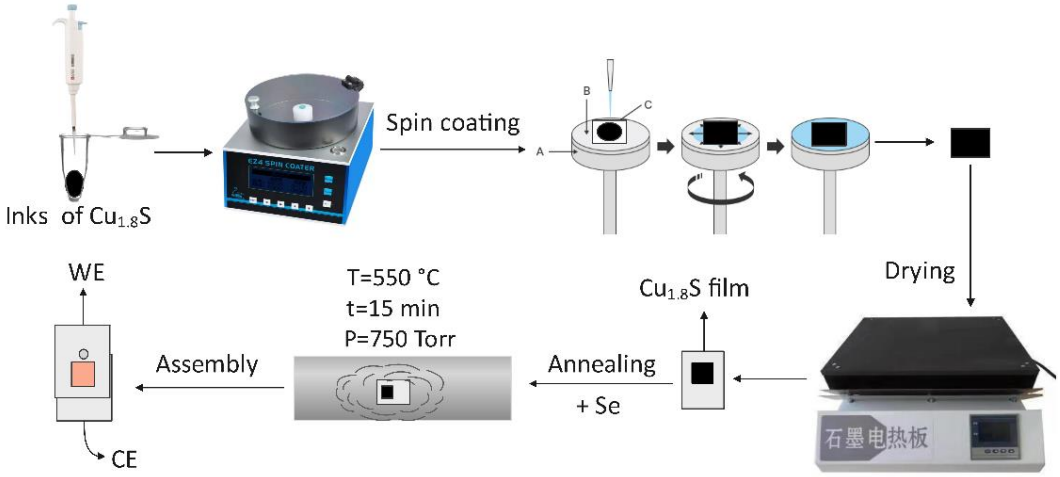

Figure S6. *Schematic diagram of the fabrication of $Cu_{1.8}S_{1-x}Se_x$ CEs.*

6.2 Optical properties

The optical absorption of the F-CS_0, F-CS_1, F-CS_2 and F-CS_3 CEs are shown in Fig. S5a. The CEs showed good absorption in the visible range. The Tauc plotting method was adopted to estimate the bandgap values of the samples. As shown in Fig. S5b, with the increasing of the selenylation degree, the bandgap decreases firstly and then increases. This indicate that proper selenylation degree can modulate the bandgap of the material [2].

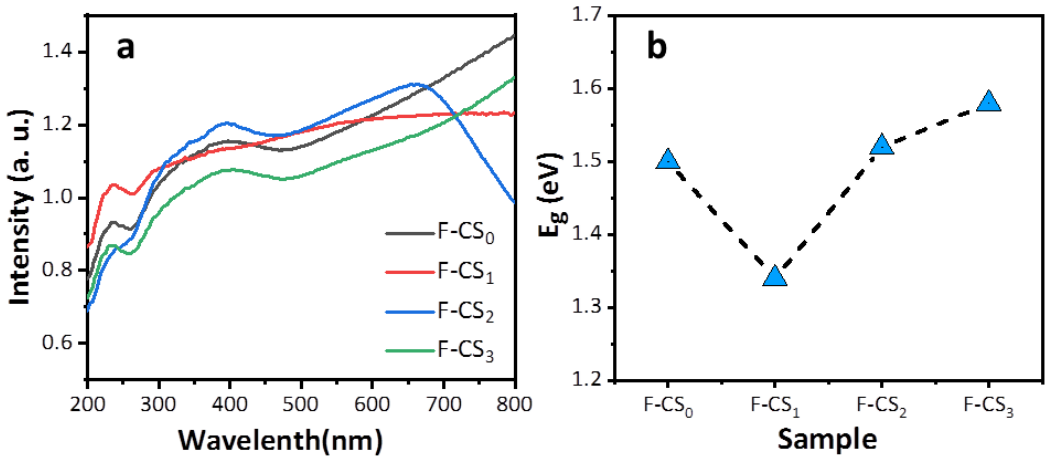

Figure S7. *Absorbance spectra (a) and bandgap of the CEs (b).*

6.3 Energy level alignment in the DSSCs

Figure.S6a-6d shows the VBM values estimated by VB-XPS. As shown in Fig. S6e, ΔE is the difference between the conduction band bottom (CBB) values of the F-CS_0, F-CS_1, F-CS_2 and F-CS_3 CEs and redox potential of the electrolyte ($E_{R/R'}$) (-4.9 eV) which can be used to evaluate the driving force for charge transfer at the CE/electrolyte interface. ΔE is in the order of F-CS_2 > F-CS_3 > F-CS_1> F-CS_0.

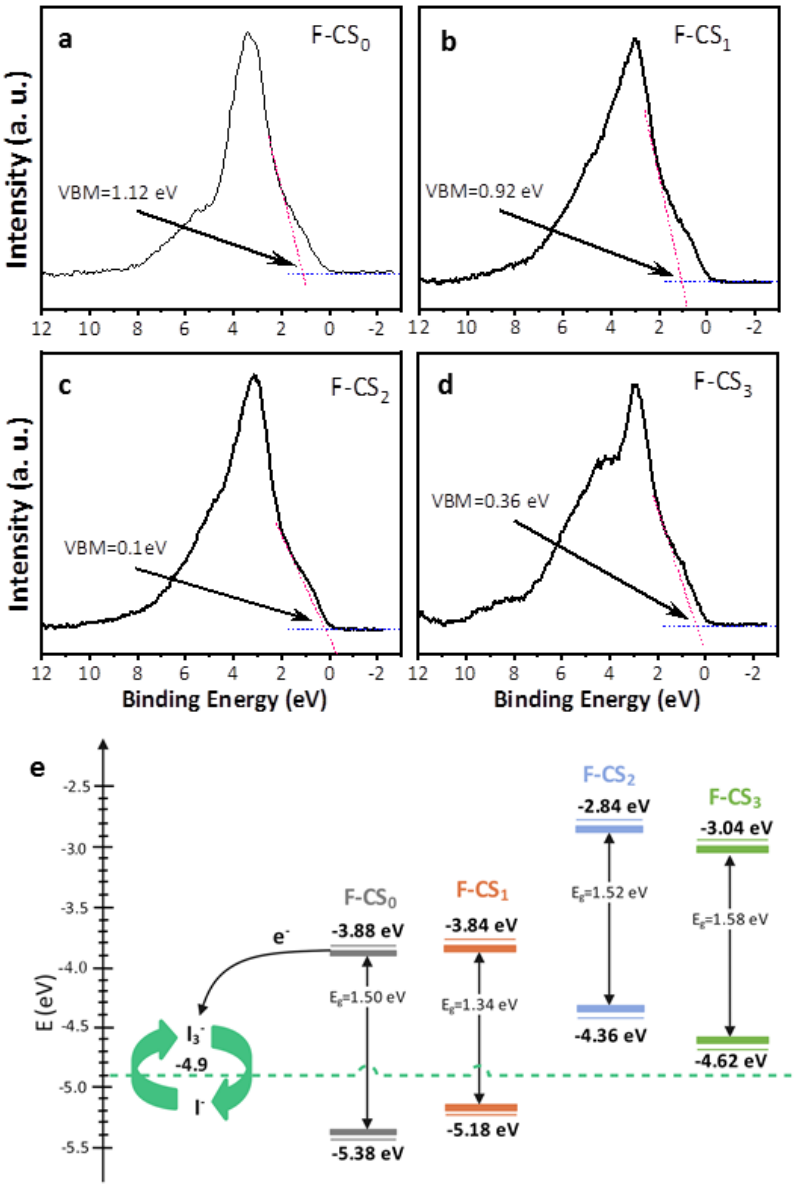

Figure S8. *VB-XPS plots of CEs (a-d) and Energy level alignment in the DSSCs (e).*

6.4 Photovoltaic performances of the DSSCs

Figure S7 shows the *J-V* curves and corresponding parameters of the DSSCs. The PCE gradually increased with increasing selenylation, and when F-CS_2 was used as CE of DSSCs, the values of both J_{sc} and *FF* improved and the PCE increased to 4.16%, which was higher than that of the $Cu_{1.8}S$ (2.87%). With a further increase in selenylation, the PCE and *FF* present a decreasing trend (F-CS_3) [3]. The PCE of F-CS_0 is lower than that of F-S_0 (3.38%), which is due to the increase in FTO conductive glass resistivity during the annealing of F-CS_0 at 550 °C [4, 5].

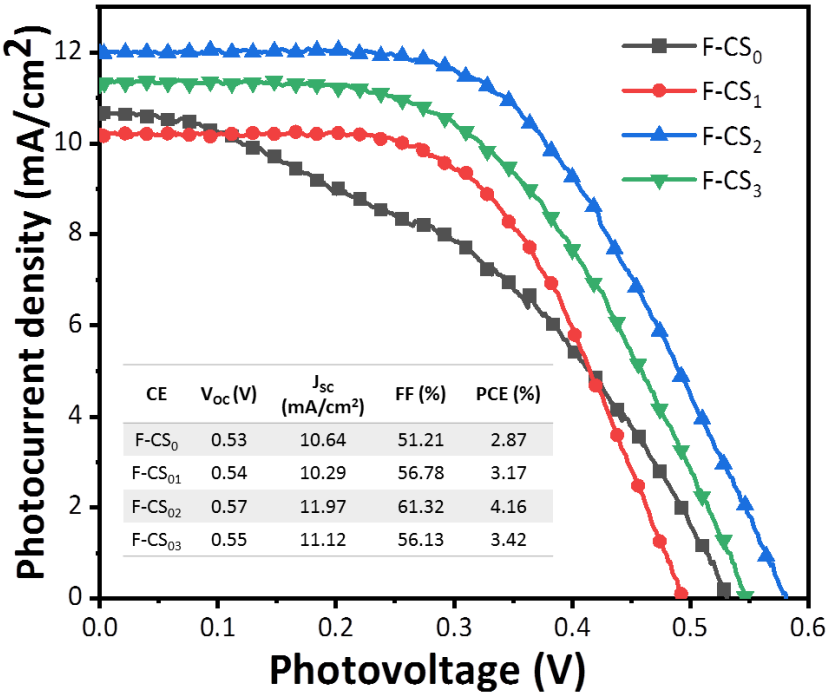

CE	V_{oc} (V)	J_{sc} (mA/cm²)	FF (%)	PCE (%)
F-CS_0	0.53	10.64	51.21	2.87
F-CS_{01}	0.54	10.29	56.78	3.17
F-CS_{02}	0.57	11.97	61.32	4.16
F-CS_{03}	0.55	11.12	56.13	3.42

Figure S9. *Photocurrent density voltage characteristics of DSSCs.*

6.5 Electrochemical characterization

The Nyquist plots of the DSSCs are shown in Fig. S8 and the parameters are summarized in Table S1. The overall decrease in R_s values after selenylation indicates

that selenylation of $Cu_{1.8}S$ can effectively improve the electrical conductivity of $Cu_{1.8}S$. The R_{ct} of F-CS_2 is the smallest among the samples, indicating that charge transfer at the F-CS_2/electrolyte interface has the highest rate compared with that in the cells with other CEs.

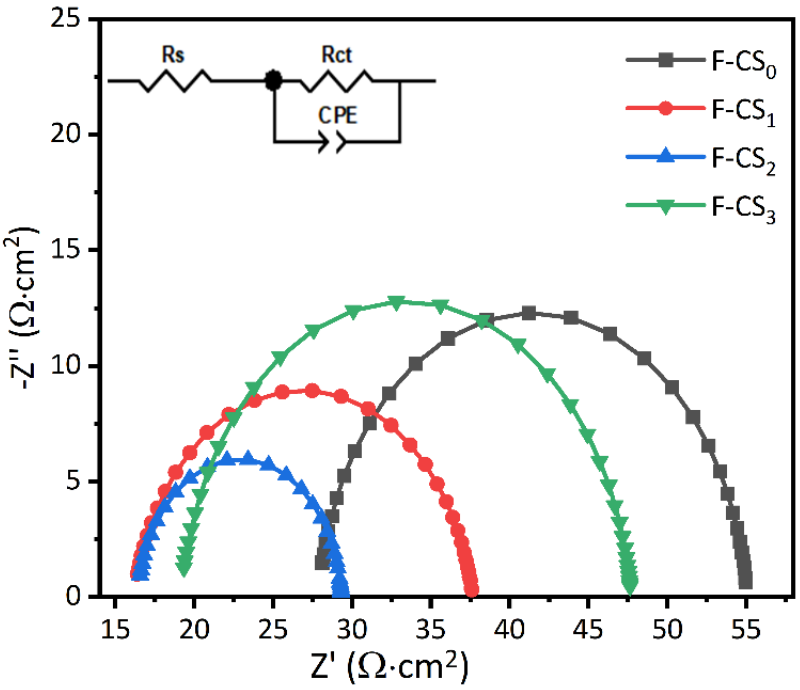

Figure S10. *EIS Nyquist plots of the DSSCs with the CEs.*

Table S1. EIS parameters extracted from Fig. S8.

CE	R_s (Ω·cm^2)	R_{ct} (Ω·cm^2)
F-CS_0	27.9	27.3
F-CS_1	16.5	21.5
F-CS_2	16.4	13.0
F-CS_3	19.2	28.5

6.6 Stability of the as-fabricated CEs

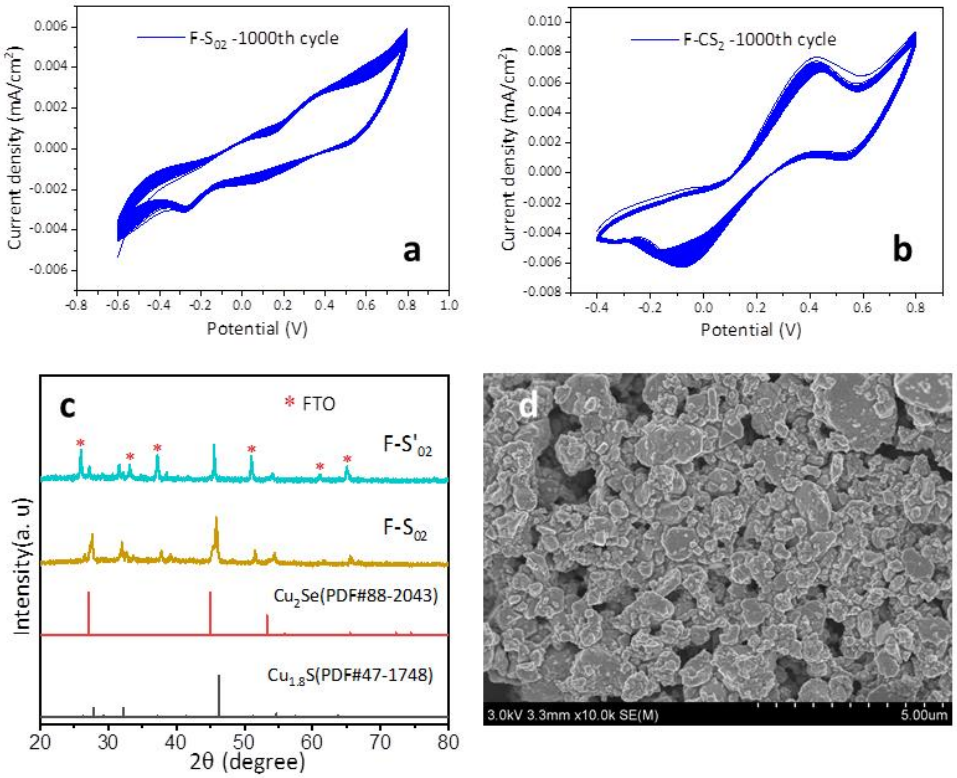

Figure S11. *CA curves of CEs (a for F-S_{02} and b for F-CS_2), XRD pattern of F-S02 before (F-S_{02}) and after 1000 CV cycles (F-S'_{02}) (c), and SEM image of F-S02 surface after 1000 CV cycles.*

References

[1] J. Liao, M. Ye, A. Han, J. Guo, Q. Liu, G. Yu, Carbon 177 (2021) 115-127.

[2] S.-H. Su, W.-T. Hsu, C.-L. Hsu, C.-H. Chen, M.-H. Chiu, Y.-C. Lin, W.-H. Chang, K. Suenaga, J.-H. He, L.-J. Li, Frontiers in Energy Research 2 (2014).

[3] J. Yang, C. Bao, J. Zhang, T. Yu, H. Huang, Y. Wei, H. Gao, G. Fu, J. Liu, Z. Zou, Chem Commun (Camb) 49 (2013) 2028-2030.

[4] K. Onoda, S. Ngamsinlapasathian, T. Fujieda, S. Yoshikawa, Solar Energy Materials and Solar Cells 91 (2007) 1176-1181.

[5] S. Ngamsinlapasathian, T. Sreethawong, S. Yoshikawa, CESolid Films 516 (2008) 7802-7806.